Magnetic order in $ErFeO_3$ single crystals studied by mean-field theory

E. E. Zubov,[1,*] V. Markovich,[2] I. Fita,[3] A. Wisniewski,[3] and R. Puzniak[3]
[1]*G. V. Kurdyumov Institute for Metal Physics, NASU, 03680 Kyiv, Acad. Vernadsky Boulevard 36, Ukraine Vasyl' Stus Donetsk National University, 021021 Vinnytsia, Ukraine*
[2]*Department of Physics, Ben-Gurion University of the Negev, P.O. Box 653, 84105 Beer-Sheva, Israel*
[3]*Institute of Physics, Polish Academy of Sciences, Aleja Lotnikow 32/46, PL-02668 Warsaw, Poland*

(Received 11 January 2019; revised manuscript received 15 April 2019; published 15 May 2019)

Recent experiments showed magnetic moment reversal and pronounced exchange-bias (EB) effect in the vicinity of the compensation temperature T_{comp} of orthoferrites $RFeO_3$ (R = Nd, Sm, Er). Although different orthoferrites exhibit diverse R-Fe interactions, T_{comp} values, and spin-reorientation temperatures, the EB field in the like manner emerges and diverges upon approaching T_{comp} and changes its sign with crossing T_{comp}. In order to explain these observations, a mean-field theory approach for the representative $ErFeO_3$ orthoferrite is proposed. The general case of two sublattices, antiferromagnet with exchange anisotropy and rare-earth–iron interactions, is considered. A small applied magnetic field appears to be a source of additional anisotropy, resulting from canting of sublattice moments. This anisotropy leads to an imbalance of free energy for two different types of magnetic domains, causing a spin jump near the T_{comp}. The suggested approach allows reproduction of magnetization reversal and main features of the coercive and exchange-bias fields observed in $ErFeO_3$.

DOI: 10.1103/PhysRevB.99.184419

I. INTRODUCTION

Basic magnetic properties of the rare-earth orthoferrites $RFeO_3$ (R is a rare-earth ion) were studied intensively 50–60 years ago and, as pointed out in the classical review of White [1], the investigated compounds exhibit great and sometimes bewildering magnetic properties. Usually, they show a similar orthorhombically distorted perovskite structure with the space group *Pnma*. At the Néel temperature T_N (between 620 and 750 K) the Fe^{3+} magnetic moments in $RFeO_3$ undergo a magnetic phase transition into a canted antiferromagnetic (AFM) state [1,2]. In some cases, a canted antiferromagnet displays also a spin-reorientation (SR) transition, comprising two second-order phase transitions within a certain temperature interval, where the spins rotate by 90° from one symmetry axis to another one [3–10]. For most orthoferrites, spins of rare-earth ions order at temperatures 2–6 K [1]. Generally, magnetization of R^{3+} ions sublattice is negligible above 100 K. It should be noted that owing to a strong AFM coupling between R^{3+} and Fe^{3+} ions, the compensating paramagnetic moment of R spins in $RFeO_3$ is oriented oppositely to the weak ferromagnetic (FM) moment of canted Fe spins. Due to this mechanism, the Er, Nd, and Sm orthoferrites exhibit specific compensation temperatures T_{comp} = 45, 9.2, and 4.8 K, respectively [1,7,8], at which the two opposite moments cancel each other so that the net magnetization vanishes, and below T_{comp} the FM moment is aligned oppositely to the moderate applied magnetic field, demonstrating a negative magnetization. The first-principles density-functional theory calculations confirmed such scenario in $NdFeO_3$ [11].

The $ErFeO_3$ orthoferrite is a representative of the $RFeO_3$ family which demonstrates the following sequence of transitions with decreasing temperature, typical for some rare-earth orthoferrites: antiferromagnetic phase transition, SR transition, and finally long-range ordering of the Er^{3+} moments [1–4]. Below $T_N \approx 636$ K, the Fe^{3+} ions order into four sublattices, which are antiferromagnetically coupled. The presence of the Dzyaloshinskii-Moriya (DM) interaction induces small canting between these sublattices, leading to a macroscopic magnetization with a weak FM moment along the c axis. With further cooling below 100 K the Fe^{3+} spins start spontaneous rotation in the ac plane at $T_1 = 97$ K and end this process at $T_2 = 88$ K; the FM moment rotates from the orthorhombic c axis towards the a axis [9,10]. With further lowering of temperature, $ErFeO_3$ exhibits a magnetic compensation with the highest T_{comp} among the $RFeO_3$ compounds. Finally, the long-range AFM order of Er^{3+} spins develops below 4.3 K [12,13]. It should be noted that $ErFeO_3$ shows quite remarkable behavior in the vicinity of $T_{comp} = 45$ K. In particular, temperature dependence of magnetization shows the "butterfly pattern" behavior, characteristic of the first-order transition around the T_{comp} [14]. Moreover, the coercive field H_C, defined as the position of the magnetization jump, diverges for $T \to T_{comp}$ [15].

Previously, we have shown that $ErFeO_3$ orthoferrite exhibits a versatility of the exchange-bias (EB) behavior [8]. The EB appears in the vicinity of the T_{comp}, increases upon approaching T_{comp}, and changes sign across T_{comp}. The EB was found to depend crucially on thermal history. It was suggested that the negative EB is compatible with the equilibrium spin configuration and the positive one with the metastable state [8]. More recently, we studied the EB effect in two other compensated ferrimagnets (fM) of the $RFeO_3$ family (R = Nd, Sm) and we have shown that there are several

*eezubov@ukr.net

important features which are common for all studied compensated orthoferrites [7]. In particular, it was revealed that despite the different strength of the R-Fe interactions, $T_{\rm comp}$ values, and spin-reorientation temperatures in these orthoferrites, the EB field similarly emerges and diverges upon approaching $T_{\rm comp}$ and changes sign with crossing $T_{\rm comp}$.

There is a considerable number of investigations of magnetic structures in orthoferrites $R\mathrm{FeO_3}$. In particular, Bertaut symmetry analysis showed all possible magnetic structures in orthoferrites [16]. Many studies were devoted to theoretical interpretations of the observed properties. As a rule, a phenomenology approach in the framework of Landau theory was used [17,18]. Methods of quantum Hamiltonian were also applied in some works [19,20]. Unfortunately, in this case many parameters and classic spin representation are used, which may lead one astray in the interpretations of the experimental results. In this paper, more exact analysis is reported, especially in the context of the phenomena observed for compensated fM, such as ultrafast spin switching, spin-reorientation transition, field- and temperature-induced sharp magnetization reversal, negative magnetization, and the positive and negative exchange-bias effect [7,8,21–26]. Some related perovskites $M\mathrm{FeO_3}$, where M is transition metal, show such multiferroic properties as ferroelectric (FE) polarization, structural antiferrodistortion (AFD), and ferro- and antiferromagnetic ordering. Studies of the thermodynamics, with complicated systems of order parameters, using combined quantum-mechanical and phenomenological theory, were performed in order to find the Landau-Ginzburg-Devonshire free energy [27–29]. Based on experimental data for $\mathrm{BiFeO_3}$, it allows description of a specific structure of AFD-FE domain walls, multiferroic phase diagram, ferroelectric polarization, AFD tilt, and so on. Also, there is a correlation between magnetic and possible AFD order in $R\mathrm{FeO_3}$ like for $M\mathrm{FeO_3}$. In particular, first-principles calculations show [30] that induced magnetization is proportional to a value of anti-phase tilting of oxygen octahedra for staggered AFM structure. Thus, a vector parameter of the DM interaction is the difference between AFD pseudovectors of the nearest neighbors. These recent findings stimulated studies aimed at improving understanding of magnetic properties of orthoferrites.

Taking $\mathrm{ErFeO_3}$ as an example, we present a more rigorous mean-field theory of magnetism in orthoferrites based on quantum spins of iron and rare-earth ions. This theoretical approach allows one to analyze the origin of spin-reorientation transition, compensation point, and to understand steplike spin overturn attributed to the additional anisotropy fields at a small total magnetization. The structure of the paper is as follows. In Sec. II, the starting anisotropic Hamiltonian of the Fe^{3+} and Er^{3+} systems is formulated. The simple form, which accounts for a weak anisotropic Heisenberg Hamiltonian with an easy axis directed along the a axis, was applied. The single-ion anisotropy was neglected since for Er^{3+} the effective spin $\sigma = 1/2$ was supposed and an orbital S state for Fe^{3+} was considered, and DM anisotropy in the xz plane with single parameter d along the y axis only was taken into account. A range of temperatures significantly above the ordering temperature of the rare-earth ions was considered. That is why the effective Weiss field at the rare-earth sites is caused by iron subsystem only. In Sec. III, the results of numerical calculations of total mean spin, free energy, and its analysis at temperature $T=0$ are presented. In Sec. IV, free energy, phase transitions, and magnetic structure were analyzed for finite temperatures. Moreover, a possible reason of the exchange-bias effect is proposed in Sec. V. Finally, conclusions are presented in regard to the most typical experimental data.

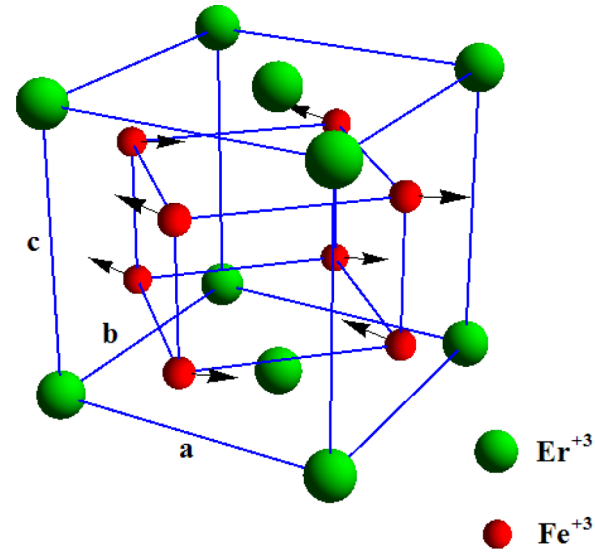

FIG. 1. Magnetic structure of Er orthoferrite at $T_{\rm SR} < T < T_{\rm N}$ with the space group *Pbnm*.

II. MAGNETIC HAMILTONIAN OF THE IRON-ERBIUM SYSTEM IN $\mathrm{ErFeO_3}$ ORTHOFERRITE

In accordance with Bertaut analysis, there are four Fe^{3+} and four Er^{3+} magnetic sublattices in $\mathrm{ErFeO_3}$ orthoferrite [16]. Fortunately, a small deviation of the sublattice moments along the y axis allows one to consider a simple two-sublattice model for Fe^{3+} subsystem as a good approximation. The erbium subsystem is in paramagnetic state. In Fig. 1, the magnetic structure of the orthoferrite at $T_{\rm SR} < T < T_{\rm N}$ with the space group *Pbnm* is shown. In the general case, the total magnetic Hamiltonian is written as [19]

$$\hat{H} = \sum_{i_1 j_2} j_{12} \boldsymbol{S}_{i_1} \boldsymbol{S}_{j_2} + \sum_{i_1 j_2} b_{12} S^z_{i_1} S^z_{j_2} + \sum_{i_1 j_2} \boldsymbol{D}_{12} \left[\boldsymbol{S}_{i_1} \times \boldsymbol{S}_{j_2}\right] + \sum_{ik\alpha} \tilde{j}_\alpha S^\alpha_i \sigma^\alpha_k, \tag{1}$$

where the parameters j_{12} and b_{12} determine the isotropic and anisotropic terms of the symmetric exchange Fe^{3+}-Fe^{3+} interactions. Here, $\boldsymbol{D}_{12} \| b$ and $\tilde{j}_\alpha$ are parameters of the antisymmetric DM and isotropic exchange Fe^{3+}-Er^{3+} interactions, respectively. The interactions Er^{3+}-Er^{3+} are also assumed to be weak.

On this basis, it is possible to write a total mean-field Hamiltonian with mean iron and erbium spins $\langle S_{i\alpha} \rangle$ and $\langle \sigma_\alpha \rangle$ along the α direction in the i-th sublattice, respectively, in the form

$$\hat{H}_0 = \hat{H}_{0\rm Fe} + \hat{H}_{0\rm Er}. \tag{2}$$

TABLE I. Parameters used in calculations of magnetic structure of $ErFeO_3$.

Parameter	Designation	Numerical value or range	Ref. or note
Fe^{3+}-Fe^{3+} ISLEI	$j_{12}(0) = z_1 j_{12}$	97–109 (K)	Fit
Anisotropic part of the ISLEI Fe^{3+}-Fe^{3+}	$B_{12} = z_1 b_{12}$	−(0.29–0.33) (K)	Fit
Anisotropic DM Fe^{3+}-Er^{3+} ISLEI	$d_{12}(0) = z_1 D_{12}$	5.6–6.3 (K)	Fit
Anisotropic Fe^{3+}-Er^{3+} exchange	$\tilde{J}_x(0) = z_2 \tilde{j}_x$	162–182 (K)	Fit
interaction in α direction	$\tilde{J}_z(0) = z_2 \tilde{j}_z$	19–22 (K)	Fit
Number of the nearest Fe^{3+} neighbors	z_1	6	
for Fe^{3+} and Er^{3+} subsystem	z_2	8	
Néel temperature	T_N	636 (K)	[2]
Spin-reorientation transition temperature	T_{SR}	88–97 (K)	[9,10]
Compensation temperature	T_{comp}	45 (K)	[13]
g factors of Fe^{3+} and Er^{3+} ions	g_{Fe}, g_{Er}	2, 1.2	[2,32]

The details of $\hat{H}_0$ derivation are given in Supplemental Material, Appendix A [31]. For N ions of each Fe^{3+} sublattice,

$$\hat{H}_{0Fe} = \sum_{i_1}^{N} \left(\tilde{H}_{2x} S_{i_1 x} + \tilde{H}_{2z} S_{i_1 z}\right) + \sum_{i_2}^{N} \left(\tilde{H}_{1x} S_{i_2 x} + \tilde{H}_{1z} S_{i_2 z}\right) - 2d_{12}(0) N\{\langle S_{1z}\rangle\langle S_{2x}\rangle - \langle S_{1x}\rangle\langle S_{2z}\rangle\} - 2N\{J_{12}(0)\langle S_{1x}\rangle\langle S_{2x}\rangle + [J_{12}(0) + B_{12}]\langle S_{1z}\rangle\langle S_{2z}\rangle\}, \tag{3}$$

where $J_{12}(0)$, B_{12}, and $d_{12}(0)$ are indirect exchange interaction, exchange anisotropy between iron ions from the first and the second sublattice [intersublattice exchange interaction (ISLEI)], and the y component of vector parameter of DM interaction, respectively. All parameters used in the next calculations for magnetic structure are presented in Table I. For $2N$ ions of Er^{3+}, interacting with the nearest N iron ions,

$$\hat{H}_{0Er} = \sum_{j}^{2N} (\tilde{H}_x \sigma_{jx} + \tilde{H}_z \sigma_{jz}) - N\{\tilde{J}_x(0)(\langle S_{1x}\rangle + \langle S_{2x}\rangle)\langle\sigma_x\rangle + \tilde{J}_z(0)(\langle S_{1z}\rangle + \langle S_{2z}\rangle)\langle\sigma_z\rangle\}, \tag{4}$$

where $\tilde{J}_\alpha(0)$ is a parameter of indirect exchange interaction between iron and erbium ions (R-Fe interaction) in the α-th direction. Neglecting the interactions between erbium ions, the effective exchange fields $\tilde{H}_{i\alpha}$ at the iron sites with $i = 2$ or 1 for the first or the second sublattices, respectively, along the α direction in applied field $\mathbf{H} = (H_x,\ H_z)$ are expressed as

$$\tilde{H}_{i\alpha} = 2[J_{12}(0) + \delta_{\alpha z} B_{12}]\langle S_{i\alpha}\rangle \pm 2d_{12}(0)\langle S_{i\beta}\rangle + \tilde{J}_\alpha(0)\langle\sigma_\alpha\rangle - g_{Fe} H_\alpha, \tag{5}$$

where $\delta_{\alpha\beta}$ is the Kronecker symbol and upper and lower signs correspond to $i = 1$, $\alpha = x \| a$ or $i = 2$, $\alpha = z \| c$ and $i = 1$, $\alpha = z$ or $i = 2$, $\alpha = x$, respectively, $\alpha \neq \beta$, and g_{Fe} is the g factor of Fe^{3+} ion. Here and further, for simplicity, we set Bohr magneton $\mu_B = 1$. For the rare-earth subsystem,

$$\tilde{H}_\alpha = \tilde{J}_\alpha(0)(\langle S_{1\alpha}\rangle + \langle S_{2\alpha}\rangle) - g_{Er} H_\alpha, \tag{6}$$

where g_{Er} is the g factor of Er^{3+} ions. For exchange interactions, in what follows, approximation of the nearest neighbors is used. One can set $\langle \tilde{S}_z\rangle = S$ for temperatures $T \ll T_N$ and spin $S = 5/2$ for Fe^{3+}. Also, applied magnetic field $\mathbf{H}$ is orthogonal to the AFM axis L, i.e., in the general case $H_x = -H\sin\alpha$ and $H_z = H\cos\alpha$.

Apparently, for $J_{12}(0) > 0$ and $\tilde{J}_\alpha(0) > 0$, the interactions are antiferromagnetic. Furthermore, the parameter $d_{12}(0) > 0$ corresponds to positive canting angles. Strictly speaking, magnetic axes x, y in this compound do not coincide with crystallographic a and b axes. However, for simplicity, this discrepancy is neglected. That is why the parameter $B_{12} < 0$ corresponds to the ground state of easy-axis type along the a direction for iron sublattice mean spins.

In spite of its simple form, the Hamiltonian (2) describes the main peculiarities connected with canting of magnetic moment of iron sublattices, SR transition, and compensation point. It is easy to diagonalize Hamiltonian (2) and to find ground state, magnetic structure at different temperatures, and critical points of the phase transitions (see Supplemental Material, Appendix B [31]).

Let us enter the next designation: $d = d_{12}(0)/J_{12}(0)$, $b = B_{12}/J_{12}(0)$, $h_\alpha = H_\alpha/2J_{12}(0)$, $\gamma_x = J_{12}(0)/\tilde{J}_x(0)$, and $\gamma_z = J_{12}(0)/\tilde{J}_z(0)$. Then the equation for canting angle θ of the Fe^{3+} sublattice magnetic moment relatively AFM axis L (see Appendix B in Ref. [31]) is written as

$$\sin(2\theta) + \frac{1}{2} b[\sin(2\theta) - \sin(2\alpha)] - d\cos(2\theta) + \frac{1}{2S}\langle\sigma\rangle\left(\frac{1}{\gamma_z}\cos(\theta+\alpha)\cos(\varphi) - \frac{1}{\gamma_x}\sin(\theta+\alpha)\sin(\varphi)\right) - \frac{g_{Fe} h}{S}\cos(\theta) = 0, \tag{7}$$

where the dimensionless applied field $h = H/2J_{12}(0)$. Here, the angle φ determines the quantum axis direction for Er^{3+} spin relative to the z axis. It is related to the angle α by the equation (see Appendix B, Eq. (B7), in Ref. [31])

$$\tan\varphi = -\frac{\gamma_z}{\gamma_x}\frac{S\sin(\theta) - g_{Er}\gamma_x h}{S\sin(\theta) - 2g_{Er}\gamma_z h}\tan\alpha. \tag{8}$$

For introduced parameters, the remaining equation takes the form

$$\langle\sigma\rangle = -\frac{1}{2}\tanh\frac{\tilde{\tilde{h}}(\alpha)}{2\tilde{T}}, \tag{9}$$

where the reduced temperature $\tilde{T} = \frac{T}{2J_{12}(0)}$. The effective exchange field for Er^{3+} sublattice is determined as follows:

$$\tilde{\tilde{h}}(\alpha) = \sqrt{\sin^2(\alpha)\left(\frac{S}{\gamma_x}\sin(\theta) - g_{\mathrm{Er}}h\right)^2 + \cos^2(\alpha)\left(\frac{S}{\gamma_z}\sin(\theta) - g_{\mathrm{Er}}h\right)^2}, \tag{10}$$

which means that $\langle\sigma\rangle$ depends on α. The simplified system of Eqs. (7)–(10) allows us to solve rigorously the spin-reorientation transition problem. Thus, the expressions for single-site free energy F in units $2J_{12}(0)$ for $T \ll T_{\mathrm{N}}$ we write as follows:

$$\tilde{F}(\alpha_i) = -\frac{1}{2}S^2\left\{\cos(2\theta) + d\sin(2\theta) - \frac{b}{2}[\cos(2\alpha_i) - \cos(2\theta)]\right\} - \tilde{T}\ln\left[2\cosh\left(\frac{\tilde{\tilde{h}}(\alpha_i)}{2\tilde{T}}\right)\right] - g_{\mathrm{Fe}}Sh\sin(\theta). \tag{11}$$

A ground state of the rare-earth orthoferrite and phase transition in the ordered state are discussed in the next section.

III. SPIN-REORIENTATION TRANSITION AND ENERGY OF THE GROUND STATE

For axis L along a and c, respectively, with fixed γ_i, it is easy to find from Eq. (11) at $T = 0$ that

$$\begin{aligned}\tilde{F}(0) &= -\frac{1}{2}S^2\{\cos(2\theta_z) + d\sin(2\theta_z) - b\sin^2\theta_z\} \\ &\quad - \frac{1}{2\gamma_z}S\sin\theta_z \\ \tilde{F}(\pi/2) &= -\frac{1}{2}S^2\{\cos(2\theta_x) + d\sin(2\theta_x) + b\cos^2\theta_x\} \\ &\quad - \frac{1}{2\gamma_x}S\sin\theta_x.\end{aligned} \tag{12}$$

Here, the canting angle θ_i is determined by Eq. (7), i.e.,

$$(2+b)\sin(2\theta_i) - 2d\cos(2\theta_i) - \frac{1}{2\gamma_i S}\cos(\theta_i) = 0. \tag{13}$$

In the case $\gamma_x = \gamma_z$, the value $\theta_x = \theta_z$ and the difference takes the form

$$\tilde{F}(0) - \tilde{F}(\pi/2) = \tfrac{1}{2}bS^2. \tag{14}$$

Thus, an easy axis is along the a direction ($L\|a$) at $b < 0$ and for $b > 0$ the ground state is with $L\|c$. It is important to point out that the direction L does not depend on isotropic R-Fe exchange interaction, i.e., spin-reorientation transition is possible only in a case of changing the sign of b. One can say, in the framework of the considered model, that only transition $\Gamma_4(G_x, F_z) \to \Gamma_2(G_z, F_x)$ may occur in R-Fe system. The SR transition indeed occurs in $ErFeO_3$ at T_{SR} of about 100 K. This phenomenon takes place due to anisotropy of R-Fe interaction. Moreover, the strong anisotropy only allows for a spin reorientation for $b < 0$ since otherwise the ground state with easy axis along the a direction occurs for all temperatures below the Néel temperature T_{N} (see approval in Appendix B of Ref. [31]).

The influence of R-Fe exchange and DM interaction on canting angle of Fe^{3+} of sublattice magnetic moments is presented in Fig. 2, containing the results obtained by numerical solution of Eq. (13). One can see that anisotropy of the Heisenberg interaction influences θ weakly. Contrary to that, the anisotropy of the R-Fe interactions, γ_x, plays an essential role in realization of balanced angle of canting. The apparent increase of θ with increasing Dzyaloshinskii-Moriya interaction is noticed, although its influence is not strong. At $\gamma_x \to \infty$ the angle $\theta \to \theta_\infty$, where θ_∞ is determined by Eq. (B18) in Appendix B of Supplemental Material [31].

IV. THERMALLY INDUCED SPIN REORIENTATION, COMPENSATION POINT, AND CRITICAL TEMPERATURE

The critical temperature T_{N} as a function of d is presented in Fig. 3. One can see that T_{N} increases with increasing canting angle. The Heisenberg anisotropy influences T_{N} only weakly. Ordinary result $T_{\mathrm{N}} = \frac{2}{3}S(S+1)J_{12}(0)$ for a two-sublattice isotropic antiferromagnet is fulfilled at $d = 0$. In this case, the T_{N} does not depend on parameters γ_i and b.

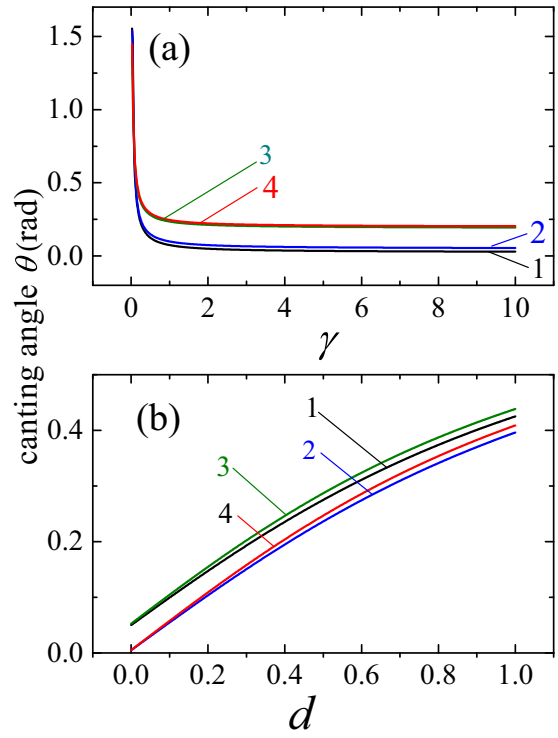

FIG. 2. Canting angle as a function of R-Fe exchange γ (a) or Dzyaloshinskii-Moriya interaction d (b) for parameters: (a) $b = -0.001$ and $d = 0.05, 0.1, 0.4$ (curves 1–3, respectively) and $d = 0.4$, $b = -0.1$ (curve 4); (b) $b = -0.001$ and $\gamma_x = 1, 10$ (curves 1 and 2, respectively) and $b = -0.1$, $\gamma_x = 1, 10$ (curves 3 and 4, respectively).

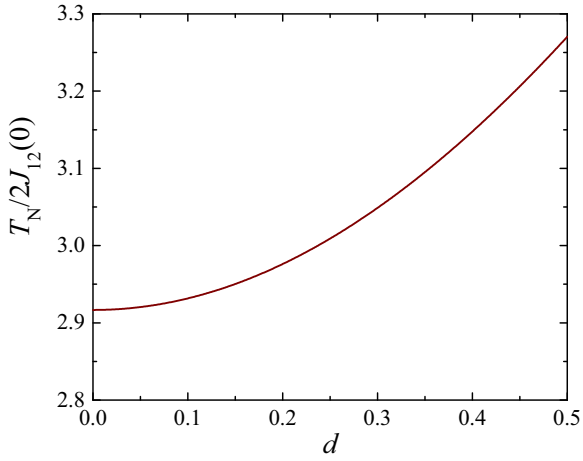

FIG. 3. Dependence of the Néel temperature T_N of the phase transition order-disorder on Dzyaloshinskii-Moriya parameter d with $\gamma_z = 10$ and $b = -0.06$.

In order to find the temperature dependence of the total magnetic moment M_{tot} and temperature of the SR (T_{SR}), the relation that works well in orthoferrites for temperatures $T \ll T_N$ was used. In this case, the free energy is expressed as in Eq. (11). To find θ_i and $\langle\sigma\rangle$ it is necessary to solve the system of equations (7) and (9). The SR temperature T_{SR} is determined as a temperature at which the difference of free-energy values (11) for fixed directions of axis L, i.e., for $\alpha = 0$ and $\alpha = \pi/2$, is equal to zero. Unfortunately, there is no analytic form for T_{SR} and the one is calculated numerically. The dependence $\tilde{T}_{SR}$ on anisotropy R-Fe exchange interaction parameter γ_x, at $\gamma_z = 5$, $b = -0.003$, and $d = 0.058$, is presented in Fig. S3 in Appendix C of Ref. [31]. One can see that $\tilde{T}_{SR}$ decreases with increasing γ_x, i.e., with disappearance of the anisotropy when $\tilde{J}_x(0) > \tilde{J}_z(0)$ and $\tilde{J}_x(0) \to \tilde{J}_z(0)$. The temperature dependences of free energy for different γ_x values at $h = 0$ for Fe^{+3} total magnetic moment along c ($\alpha = 0$) and a ($\alpha = \pi/2$) directions are presented in Fig. S4 in Appendix C of Ref. [31]. Also, the decrease of T_{SR} with increasing R-Fe exchange anisotropy is observed. It appears that the difference in R-Fe exchange anisotropy is a key factor determining a significant difference in values of T_{SR} for various orthoferrites. It is known that $SmFeO_3$ orthoferrite exhibits SR transition at temperature $T_{SR} \approx 480$ K, while for both Nd and Er orthoferrites with weaker anisotropy this transition occurs at around 100 K [11,22,23].

In the low-temperature limit $T \ll T_N$, one can write the following equations for components $\langle S_{i,tot}\rangle$ of the total mean spin $\langle \mathbf{S}_{tot}\rangle$:

$$\langle S_{x,tot}\rangle = -g_{Fe} S \sin(\alpha)\sin(\theta) + g_{Er}\sin(\varphi)\langle\sigma\rangle$$
$$\langle S_{z,tot}\rangle = g_{Fe} S \cos(\alpha)\sin(\theta) + g_{Er}\cos(\varphi)\langle\sigma\rangle, \qquad (15)$$

where φ, θ, and $\langle\sigma\rangle$ are determined by Eqs. (7)–(10). It appears that the canting angle θ is a function of α (see Fig. 4) and $\varphi = -\alpha$ for $\alpha = \alpha_i$. In what follows the total magnetic moment $M_{tot}(\alpha_i, \tilde{T})$ of erbium orthoferrite is expressed (in Bohr magnetons) as

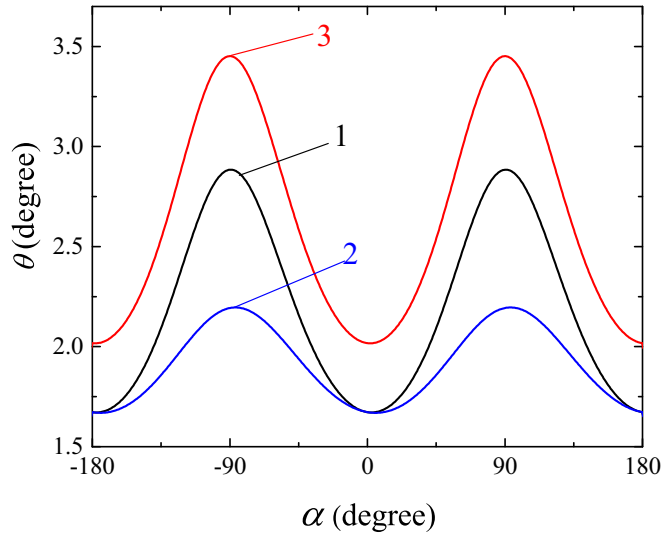

FIG. 4. Angular dependence of canting angle θ for $b = -0.003$ and $\gamma_z = 5$ for parameters $d = 0.058$, $\gamma_x = 0.6$, and $\gamma_x = 0.8$ (curves 1 and 2, respectively) and $d = 0.7$ and $\gamma_x = 0.6$ (curve 3).

$$M_{tot}(\alpha_i, \tilde{T}) = \pm\left[g_{Fe}\sin(\theta)S - \frac{g_{Er}}{2}\tanh\left(\frac{\sin(\theta)S}{2\gamma_i\tilde{T}}\right)\right] \qquad (16)$$

for $h = 0$, $\alpha_z = 0$, and $\alpha_x = \pi/2$, upper and lower sign, respectively. The g-factor values pointed out for Fe^{3+} and Er^{3+} (see Table I) correspond to the experimentally observed effective numbers of Bohr magnetons 5.92 and 9.58 [2], respectively.

The temperature dependences of total magnetic moment in erbium orthoferrite are presented in Fig. 5 for different values of R-Fe exchange interactions along the x axis. One can see that only for strong anisotropy $\gamma_x \leqslant 1$ of R-Fe exchange interaction the SR occurs, manifesting as a jump of $M_{tot}(\alpha_i, \tilde{T})$. It can be seen from Fig. 5 that for the weakest

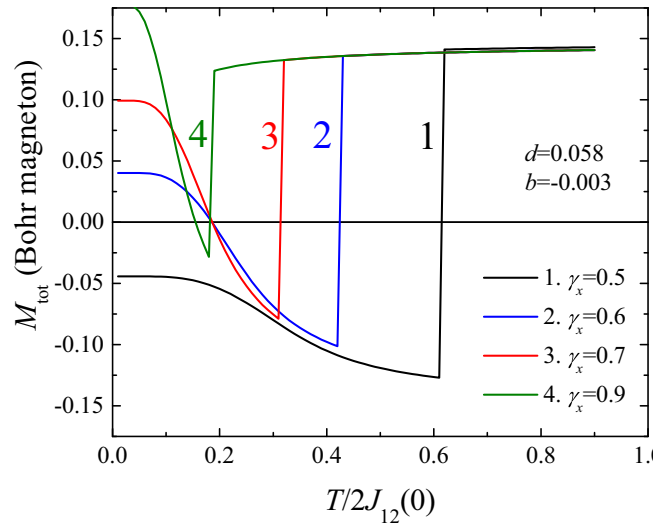

FIG. 5. Temperature dependences of total magnetic moment for different values of the R-Fe exchange along the c axis.

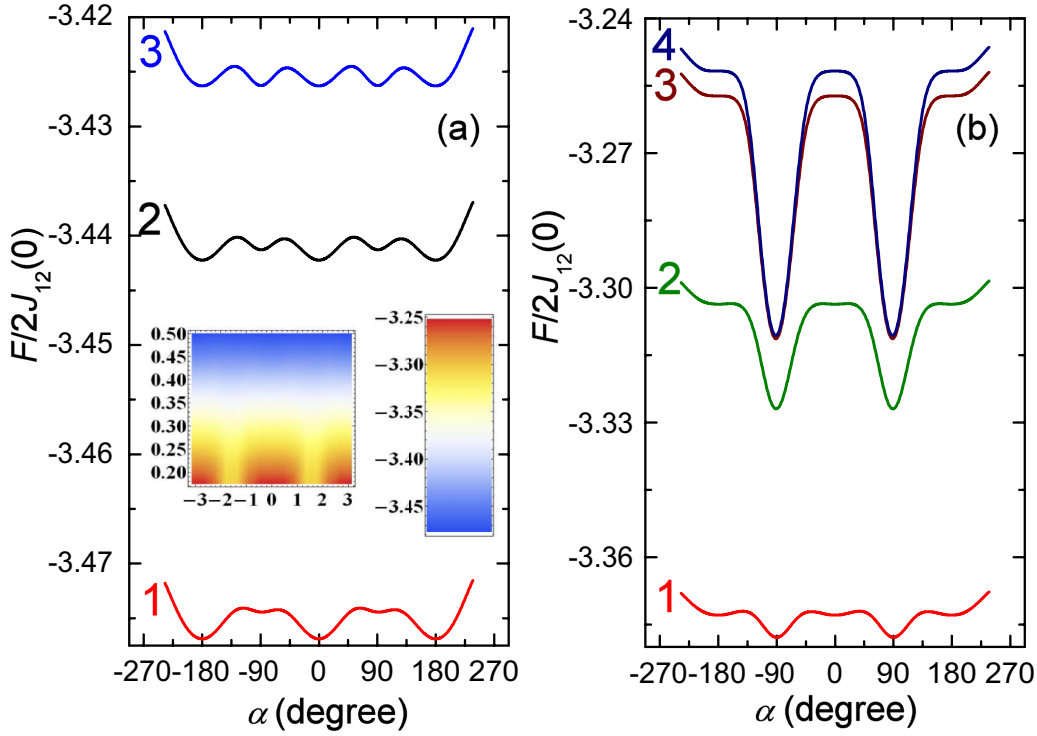

FIG. 6. Angular dependence of the free energy F for $b = -0.003$, $d = 0.058$, $\gamma_z = 5$, and $\gamma_x = 0.6$ at temperatures $\tilde{T}$: (a) 0.5, 0.45, and 0.427 (curves 1–3, respectively); (b) 0.35, 0.25, 0.183, and 0.175 (curves 1–4, respectively). Inset: density plot F as a function of angle α in radians and $\tilde{T}$.

anisotropy with $\gamma_x = 0.9$ the T_{SR} tends to zero. When the SR occurs with magnetization overturn (see Fig. 5), the further temperature lowering to a value $\tilde{T}_{comp}$ gives $M_{tot}(\alpha_i, \tilde{T}_{comp}) = 0$. Thus, the magnetization reverses sign at temperature $\tilde{T}_{comp}$ named as a compensation temperature. In a similarity to T_{SR} the compensation temperature decreases in value with decrease in R-Fe exchange along the a axis (see Fig. S5 in Appendix C of Ref. [31]). At $\tilde{T} = \tilde{T}_{comp} = 0.183$ the magnetic moment $M_{tot}(\alpha_i, \tilde{T}) = 0$ is seen for $\gamma_x = 0.6$ below the temperature $\tilde{T} = \tilde{T}_{SR} = 0.426$ of spin reorientation. From Fig. 3 it follows that $\tilde{T}_N = 2.92$. For the experimental value of $T_N = 636$ K, we obtain $J_{12}(0) = 109$ K, $T_{SR} = 93$ K, and $T_{comp} = 40$ K, which is in remarkable agreement with experimentally determined temperatures of 97 and 45 K [4,8–10,15,20]. Apparently, above or below T_{SR} the ground state corresponds to an easy axis along the a ($\alpha = 0$) or c ($\alpha = \pi/2$) axis, respectively.

Let us consider the analytical expression for compensation temperature T_{comp} at which $M_{tot}(\pi/2, \tilde{T}) = 0$ [see Eq. (16)]. In such a case, it is easy to calculate T_{comp} for both low temperatures $T \ll T_N$ and small canting angles since one can set $\langle \tilde{S}_z \rangle = S$ and $\sin(\theta_T) \approx \theta_T$. From the system of Eqs. (9) and (13) for low temperature $\tilde{T}$, it follows:

$$\theta_T(2+b) = d + \frac{1}{4\gamma_x S} \tanh\left(\frac{S\theta_T}{2\gamma_x \tilde{T}}\right). \tag{17}$$

Since $M_{tot}(\pi/2, \tilde{T}) = 0$ for $\tilde{T} = \tilde{T}_{comp}$ and $\theta_T = \theta_{comp}$, we find the following equation for compensation temperature in units $2J_{12}(0)$:

$$\tilde{T}_{comp} = \frac{S\theta_{comp}}{2\gamma_x\, a \tanh\left(2S\theta_{comp}\frac{g_{Fe}}{g_{Er}}\right)}, \tag{18}$$

where the canting angle $\theta_{comp} = \frac{2\gamma_x d g_{Er}}{2\gamma_x(2+b)g_{Er} - g_{Fe}}$ (see Eq. (C2) and Fig. S5 in Appendix C in Ref. [31]). For $b = -0.003$, $\gamma_x = 0.6$ and $d = 0.058$, Eq. (18) provides the following values: $\theta_{comp} = 0.095$ rad and $\tilde{T}_{comp} = 0.183$. Thus, a sufficiently large value of the R-Fe exchange interaction for $ErFeO_3$ gives the largest T_{comp} in the series of orthoferrites. It is necessary to take into account the role of the DM anisotropy. Its value must be optimal because at small d it is difficult to induce the R-Fe effective exchange field to be competitive with Fe-Fe exchange at high temperatures. That is why $SmFeO_3$ has a high $T_{SR} = 480$ K with a low compensation point. In Fig. S5 it corresponds to a low-temperature area below T_{comp} maximum when at small d we have a drastic T_{comp} growth with increase in γ_x. The decrease of T_{comp} reflects the suppression of the DM exchange. The canting angle θ changes sign at $T_{comp} = 0$. The first-principles study [33] shows the highest oxygen octahedron tilting angles for erbium orthoferrite since Er^{3+} has the smallest ionic radius. It gives a larger value of the DM interaction parameter with larger magnetization induced by Fe^{3+} subsystem. As a result, we have the highest T_{comp} in $ErFeO_3$.

At this point it is useful to discuss the angular dependence of the free energy at temperatures near T_{SR} and T_{comp}. The angular dependences of the free energy F for different values of parameters of interactions and temperatures are shown in Fig. 6. One can see that at $\tilde{T} = \tilde{T}_{SR} = 0.427$ the free

energies for $\alpha = 0$ and $\pi/2$ practically coincide. At $T > T_{SR}$ the difference $F(0)$ and $F(\pi/2)$ is on the order of 0.44 K that corresponds to the potential barrier that matches 6.5 kOe. In temperature range close to $\tilde{T} \sim \tilde{T}_{comp} = 0.183$, the height of the potential barrier between directions of AFM axis L along the a and c axes is increased up to 160 kOe. Apparently, in this case, Fe^{3+} magnetic moments rotate in the ab plane. Correspondingly, the free-energy extrema exist only for angles $\alpha = 0, \pm\pi/2$, which points out the spin-reorientation phase transition of the first order at temperature $T = T_{SR}$.

V. MAGNETIC FIELD INDUCED EB IN $ErFeO_3$

Near the compensation point $\langle \boldsymbol{S}_{tot} \rangle \to 0$, there is a competition between anisotropy and magnetic moments induced due to inclination by magnetic field h of the Fe^{3+} sublattice. Here, we discuss the renormalized anisotropy field caused by additional canting of the Fe^{3+} magnetic moments. Indeed, $h \sim 0.0001$ is very small and corresponds approximately to 160 Oe for Fe^{3+}. Let us estimate the change of the canting angle θ caused by this value of h. From Eqs. (7), at $\alpha = \pi/2$ we obtain the difference $\Delta\theta = 5 \times 10^{-5}$ rad for $h = 0$ and 0.0001. The other parameters are the same as in figures above with $\gamma_x = 0.6$. The effective exchange field H_{eff} is ~ 200 Oe [see Eq. (C3) in Appendix C in Ref. [31]) that is on the same order of magnitude as demagnetizing fields. In order to understand the appearance of induced anisotropy, let us consider more thoroughly the change of free energy caused by applied field h near the compensation point.

Using the expression for free energy in linear approximation over θ at $\alpha \sim \pi/2$, Eq. (11) can be rewritten at low temperatures $T \ll T_N$ as

$$\tilde{F}(\alpha) = \tfrac{1}{2}S^2\{-1 - b\sin^2\alpha - 2d\theta\} - hM_{tot}(\pm\pi/2, \tilde{T}), \tag{19}$$

where $M_{tot}(\pm\pi/2, \tilde{T}) = -g_{Fe}S\theta_0 + \frac{1}{2}g_{Er}\tanh(\frac{S\theta_0}{2\gamma_x\tilde{T}})$ and θ_0 is determined by Eq. (17) at $\theta_T = \theta_0$.

It appears that at $T \sim T_{comp}$ the total magnetic moment $M_{tot}(\pi/2, \tilde{T})$ tends to zero and anisotropy contribution $\frac{1}{2}S^2b$ is finite. In this case, the anisotropy field H_A is proportional to $b/M_{tot}(\pi/2, \tilde{T})$, i.e., there is an experimentally observed increase of H_A at $T \to T_{comp}$. Also, an applied field h changes the canting angle of the Fe^{3+} sublattice moments. Thus, depending on the direction of the total Fe^{3+} sublattice moment there is a positive or negative increase of the free energy. The coercive field H_C is shifted for different types of domains as well.

Let us designate the type of domains in which magnetic field is directed against the a axis by number N2 (see Fig. 7). This type of domain corresponds to the geometry considered above. Obviously, for these domains the additional sublattice canting by magnetic field decreases the free energy. In the system, there are domains of the basic type N1 for which h is along the a axis and this direction is assigned by the experiment (see Fig. 7). Apparently, in this case in the expression (19) for free energy it is necessary to perform $h \to -h$ replacement. In fact, the field dependence $\tilde{F}(\pi/2)$ is more complicated since the canting angle θ depends on h as well.

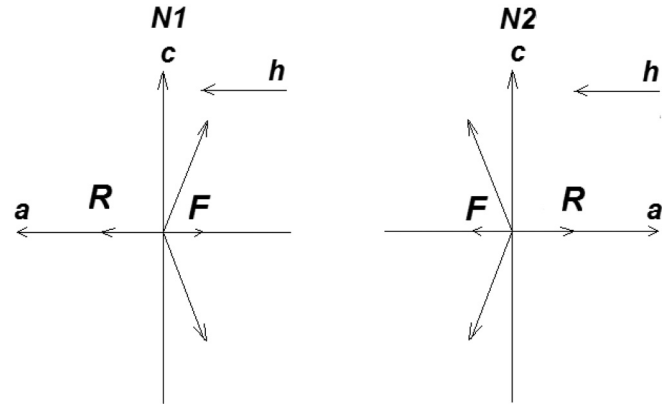

FIG. 7. Possible domains in $ErFeO_3$ at $h = 0$. Here, arrow h reflects only the direction of an applied magnetic field. Symbol F describes ferromagnetic moment from two Fe^{3+} sublattices; R is magnetic moment Er^{3+} ion for $T < T_{comp}$ ($R > F$).

In the linear approximation over h, the free energy (19) for domains N1 and N2 takes the form

$$\tilde{F}(\pm\pi/2) = \text{const} \pm hd\Delta\theta, \tag{20}$$

where $\Delta\theta = \theta - \theta_0$ is the additional magnetic bias caused by change of canting angle θ by applied field h, θ_0 is the solution of Eq. (17), and

$$\Delta\theta = \chi h. \tag{21}$$

Here, χ determines the correction to small canting angle θ_0 and is expressed as

$$\chi = \frac{g_{Fe} - \frac{g_{Er}}{8\gamma_x\tilde{T}}\left(1 - 16S^2\gamma_x^2[(2+b)\theta_0 - d]^2\right)}{S\left\{2 + b - \frac{1}{8\gamma_x^2\tilde{T}}\left(1 - 16S^2\gamma_x^2[(2+b)\theta_0 - d]^2\right)\right\}}. \tag{22}$$

Even at high temperatures χ is a sufficiently large in value $\sim\frac{g_{Fe}}{S(2+b)}$ that can shift essentially a peak of coercivity near the compensation point (see Fig. S6 in Appendix C in Ref. [31]). In experiment [8], the skewness of temperature dependences of coercive fields that may be connected with prevalence of one or another type of domain is observed.

The constant in Eq. (20) does not depend on h and is determined by angle α. It is obvious that a rotation of Fe^{3+} moments in the ac plane is thermodynamically unfavorable. It follows from Fig. 6, where the energy difference between directions along the a and c axis is of order 13 K, which is incommensurably with applied field. Apparently, the total magnetic moment rotates in the bc plane, where the anisotropic field must be essentially weak. Thus, one can write for this plane the following expression for free energy:

$$\tilde{F}(\phi) = -\tfrac{1}{2}S^2b_1\sin^2(\phi) + (M_{tot} \pm \delta\chi S^2 d)h\cos(\phi), \tag{23}$$

where ϕ is rotation angle in the bc plane and b_1 denotes the corresponding exchange anisotropy. Obviously, M_{tot} and χ depend on anisotropy parameter b, only. The parameter δ reflects a relative volume of the domains N1 and N2 with upper and lower signs, respectively. Differentiating $\tilde{F}(\phi)$ over ϕ and equating it to zero we obtain the next expression for

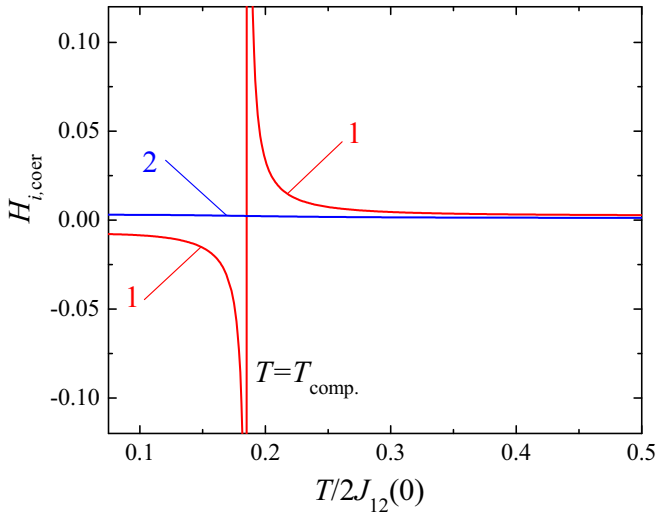

FIG. 8. Temperature dependences of the coercive fields $H_{i,\mathrm{coer}}$ for domains N1 and N2 (curves 1 and 2, respectively) for $b = -0.003$, $b_1 = -0.00005$, $d = 0.058$, $\gamma_x = 0.6$. The volume content $\delta_{+1} = 0.001$ and $\delta_{-1} = 0.999$ of domains N1 and N2, respectively.

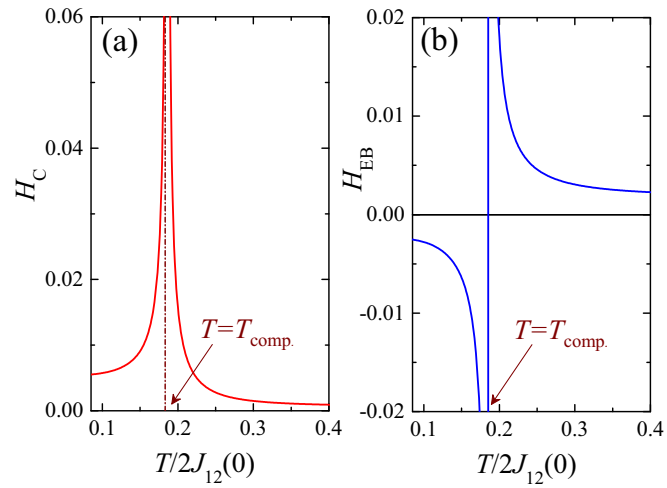

FIG. 9. Temperature dependences of the average coercive field H_{C} (a) and exchange-bias H_{EB} (b) for $b = -0.003$, $b_1 = -0.00005$, $d = 0.058$, $\gamma_x = 0.6$, $\delta_{+1} = 0.001$, and $\delta_{-1} = 0.999$.

coercive fields $H_{i,\mathrm{coer}}$ of i-th domain type:

$$H_{i,\mathrm{coer}} = \frac{S^2 b_1}{M_{\mathrm{tot}} + i\delta\chi S^2 d}, \tag{24}$$

where $i = +1$ and -1 for domains N1 and N2, respectively. Also, $M_{\mathrm{tot}} = M_{\mathrm{tot}}(\pm\pi/2)$ [see Eq. (16)].

The temperature dependences of the coercive fields $H_{i,\mathrm{coer}}$ for domains N1 and N2 are presented in Fig. 8. Experimentally observed skewness of the $H_{i,\mathrm{coer}}(T)$ [8] reflects the change of the volume ratio of domains N1 and N2. Apparently, this change has nonequilibrium character.

As defined in Ref. [8], one can determine the average coercive H_{C} and exchange-bias H_{EB} fields in the following manner:

$$H_C = \left|\frac{H_{+1,\mathrm{coer}} - H_{-1,\mathrm{coer}}}{2}\right|$$
$$H_{EB} = \frac{H_{+1,\mathrm{coer}} + H_{-1,\mathrm{coer}}}{2}. \tag{25}$$

The field H_{EB} determines the shift of the hysteresis loop center caused by existence of the two types of domains. Figures 9(a) and 9(b) show the temperature dependences of the average coercive field H_{C} and exchange-bias H_{EB}, respectively. As can be seen in Fig. 9, the sharp increase of the average coercive field and exchange bias near the compensation point are in good agreement with experimental results obtained for $ErFeO_3$ single crystals (see Ref. [8]). Obviously, only a small part of domains of type N1 is responsible for such a behavior at $T \sim T_{\mathrm{comp}}$ (see curve 1 in Fig. 9).

Let us consider the appearance of steplike overturns of magnetic moments of domains N1 and N2 near the compensation point. Indeed, above T_{comp} the basic domains are type N2 since $M_{\mathrm{tot}} > 0$ (see Fig. 7). At $h \neq 0$ nonzero magnetization appears because of rotation of the a axis in type N1 domains around the c axis through an angle 180° that is equivalent to corresponding rotation of the magnetic moments. In this case, the weak anisotropic magnetic field in the ab plane acts only. Field-induced deformation of canting angle is favorable for type N2 domains (curve 1 in Fig. 8). That is why even in a small temperature range near T_{comp} and at $T < T_{\mathrm{comp}}$ the negative magnetization due to N1 domains emerges. As the energy of deformation of canting angle becomes smaller than the energy of interaction of the total magnetic moment with applied field, spin reversal takes place. The similar situation occurs at temperature increasing from $T < T_{\mathrm{comp}}$ to $T > T_{\mathrm{comp}}$.

VI. CONCLUSIONS

For a two-sublattice antiferromagnet with exchange anisotropy and R-Fe interactions, the mean-field theory was applied. It was proved that the spin-reorientation phase transition occurs at temperature T_{SR} only for strong anisotropy of R-Fe exchange interaction. The influence of Dzyaloshinskii-Moriya and R-Fe exchange anisotropies on T_{SR} as well as compensation point has been determined. Experimentally observed steplike jumps for $ErFeO_3$ magnetization near the compensation point are explained. It was shown that magnetic exchange bias is caused by additional deformation of the canting angle of Fe magnetic sublattice in a weak applied field. Although the theory is somehow simplified, it can predict correctly significant features, such as the behavior of the average coercive field H_{C} and the exchange-bias field H_{EB}. The comparison with experiment is quite encouraging and indicates that the considered model contains the essential physics.

ACKNOWLEDGMENTS

We deeply appreciate pertinent discussions of this investigation with G. Gorodetsky. This work was partly supported by the Polish National Science Centre (NCN) Grant No. 2014/15/B/ST3/03898. E.E.Z. is thankful for support through the Fundamental Research Program funded by the Ministry of Education and Science of Ukraine, Project No. 0117U002360.

[1] R. L. White, J. Appl. Phys. **40**, 1061 (1969).
[2] D. Treves, J. Appl. Phys. **36**, 1033 (1965).
[3] G. Gorodetsky, L. M. Levinson, S. Strikman, and D. Treves, Phys. Rev. **187**, 637 (1969).
[4] H. Pinto, G. Shachar, H. Shaked, and S. Strikman, Phys. Rev. B **3**, 3861 (1971).
[5] K. P. Belov, A. K. Zvezdin, A. M. Kadomtseva, and R. Z. Levitin, Sov. Phys. Usp. **19**, 574 (1976).
[6] G. Gorodetsky and L. M. Levinson, Solid State Commun. **7**, 67 (1969).
[7] I. Fita, A. Wisniewski, R. Puzniak, E. E. Zubov, V. Markovich, and G. Gorodetsky, Phys. Rev. B **98**, 094421 (2018).
[8] I. Fita, A. Wisniewski, R. Puzniak, V. Markovich, and G. Gorodetsky, Phys. Rev. B **93**, 184432 (2016).
[9] H. Shen, Z. Cheng, F. Hong, J. Xu, S. Yuan, S. Cao, and X. Wang, Appl. Phys. Lett. **103**, 192404 (2013).
[10] Ya. B. Bazaliy, L. T. Tsymbal, G. N. Kakazei, A. I. Izotov, and P. E. Wigen, Phys. Rev. B **69**, 104429 (2004).
[11] S. J. Yuan, W. Ren, F. Hong, Y. B. Wang, J. C. Zhang, L. Bellaiche, S. X. Cao, and G. Cao, Phys. Rev. B **87**, 184405 (2013).
[12] W. G. Koehler, E. O. Wollan, and W. K. Wilkinson, Phys. Rev. **118**, 58 (1960).
[13] G. Gorodetsky, R. M. Hornreich, I. Yaeger, H. Pinto, G. Shachar, and H. Shaked, Phys. Rev. B **8**, 3398 (1973).
[14] L. T. Tsymbal, Ya. B. Bazaliy, G. N. Kakazei, and S. V. Vasiliev, J. Appl. Phys. **108**, 083906 (2010).
[15] L. T. Tsymbal, Ya. B. Bazaliy, V. N. Derkachenko, V. I. Kamenev, G. N. Kakazei, F. J. Palomares, and P. E. Wigen, J. Appl. Phys. **101**, 123919 (2007); L. T. Tsymbal, G. N. Kakazei, and Ya. B. Bazaliy, Phys. Rev. B **79**, 092414 (2009).
[16] E. F. Bertaut, in *Magnetism, Vol. 3*, edited by G. T. Rado and H. Suhl (Academic, New York, 1963), p. 150.
[17] K. P. Belov, A. K. Zvezdin, A. M. Kadomtseva, and R. Z. Levitin, *Orientation Transitions in Rare-Earth Magnetics* [in Russian] (Nauka, Moscow, 1979), pp. 320.
[18] H. Horner and C. M. Varma, Phys. Rev. Lett. **20**, 845 (1968).
[19] Y. Yamaguchi, J. Phys. Chem. Solids **35**, 479 (1974).
[20] G. Gorodetsky, S. Shtrikman, Y. Tenenbaum, and D. Treves, Phys. Rev. **181**, 823 (1969).
[21] A. V. Kimel, B. A. Ivanov, R. V. Pisarev, P. A. Usachev, A. Kirilyuk, and Th. Rasing, Nat. Phys. **5**, 727 (2009).
[22] J.-H. Lee, Y. K. Jeong, J. H. Park, M.-A. Oak, H. M. Jang, J. Y. Son, and J. F. Scott, Phys. Rev. Lett. **107**, 117201 (2011).
[23] S. Cao, H. Zhao, B. Kang, J. Zhang, and W. Ren, Sci. Rep. **4**, 5960 (2014).
[24] P. D. Kulkarni, A. Thamizhavel, V. C. Rakhecha, A. K. Nigam, P. L. Paulose, S. Ramakrishnan, and A. K. Grover, EPL **86**, 47003 (2009).
[25] K. Yoshii, Appl. Phys. Lett. **99**, 142501 (2011).
[26] X. Wang, S. Gao, X. Yan, Q. Li, J. Zhang, Y. Long, K. Ruan, and X. Li, Phys. Chem. Chem. Phys. **20**, 3687 (2018).
[27] D. V. Karpinsky, E. A. Eliseev, F. Xue, M. V. Silibin, A. Franz, M. D. Glinchuk, I. O. Troyanchuk, S. A. Gavrilov, V. Gopalan, L.-Q. Chen, and A. N. Morozovska, NPJ Comput. Mater. **3**, 20 (2017).
[28] A. N. Morozovska, E. A. Eliseev, M. D. Glinchuk, O. M. Fesenko, V. V. Shvartsman, V. Gopalan, M. V. Silibin, and D. V. Karpinsky, Phys. Rev. B **97**, 134115 (2018).
[29] E. A. Eliseev, A. N. Morozovska, C. T. Nelson, and S. V. Kalinin, Phys. Rev. **B 99**, 014112 (2019).
[30] L. Bellaiche, Z. Gui, and I. A. Kornev, J. Phys.: Condens. Matter **24**, 312201 (2012).
[31] See Supplemental Material at http://link.aps.org/supplemental/10.1103/PhysRevB.99.184419 for evident form of the mean field Hamiltonian for $ErFeO_3$ orthoferrite and corresponding unitary transform, diagonalizing this Hamiltonian. Here, it is presented the expressions for free energy and phase transition temperatures.
[32] D. L. Wood, L. M. Holmes, and J. P. Remeika, Phys. Rev. **185**, 689 (1969).
[33] H. J. Zhao, W. Ren, Y. Yang, X. M. Chen, and L. Bellaiche, J. Phys.: Condens. Matter **25**, 466002 (2013).